BIOCHEMISTRY
including biophysical chemistry & molecular biology
Article

*Biochemistry* **2010,** *49,* 793–801 793
DOI: 10.1021/bi901145a

# Binding Conformation and Kinetics of Two Pheromone-Binding Proteins from the Gypsy Moth *Lymantria dispar* with Biological and Nonbiological Ligands†

Yongmei Gong,‡ Hao Tang,§ Cornelia Bohne,§ and Erika Plettner*,‡

‡*Department of Chemistry, Simon Fraser University, Burnaby, British Columbia V5A 1S6, Canada and* §*Department of Chemistry, University of Victoria, Victoria, British Columbia V8W 3V6, Canada*

*Received July 6, 2009; Revised Manuscript Received December 16, 2009*

ABSTRACT: Pheromone-binding proteins (PBPs) in insects can bind various substances and selectively deliver the message of a signal molecule to the downstream components of the olfactory system. This can be achieved either through a ligand-specific conformational change of the C-terminal peptide of the PBP or by selectively binding/releasing the ligand. PBP may also act as a scavenger to protect the sensory neurons from saturating at high ligand doses. We have compared two PBPs from the gypsy moth (PBP1 and PBP2) and their truncated forms (TPBPs), which lack the C-terminal peptide, in this study. Stopped-flow kinetics with *N*-phenyl-1-naphthylamine (NPN) have revealed a diffusion-controlled collisional step, between PBP and NPN, after which the NPN relocates into a hydrophobic environment. This work supports the hypothesis that binding between PBPs and ligands occurs stepwise. With the method of tryptophan fluorescence quenching, we have shown different local conformational changes around Trp 37, induced by different ligands, manifested in changes of both the steric and electronic environment around the residue. Importantly, we have noticed a significant difference in the changes induced by the biological ligand (the pheromone) and nonbiological ligands. Therefore, we hypothesize that PBP may serve a different function in each kinetic step, displaying a unique P·L conformation.

Pheromone-binding proteins (PBPs)[1] play an important role in pheromone detection in insects. They are soluble proteins secreted in the sensillum lymph surrounding the olfactory neurons in the sensory hairs (sensilla). PBPs are specialized members of the insect odorant-binding protein (OBP) superfamily, and they are categorized into three groups by their lengths: the long-chain PBPs (~160 aa), the medium-chain PBPs (~120 aa), and the short-chain PBPs (~110 aa) (*1*). The major difference is in the length of their C-terminal segments, which are thought to influence ligand binding. Our group has been working on the two PBPs from the gypsy moth *Lymantria dispar*, LdisPBP1 and LdisPBP2 (PBP1 and PBP2 from here on). Both of them fall into the first group together with other PBPs from lepidopterans, such as BmorPBP from *Bombyx mori* (the silk moth) and ApolPBP from *Antheraea polyphemus* (wild silk moth). The long-chain PBPs have been proposed to involve a dramatic conformational change in the C-terminal segment from a random coil to a structured helix to release the bound ligand when approaching the negatively charged membrane of the neuron (*2*−*4*). While this is not the case for the other two classes of PBPs, recent research on medium-chain PBPs has revealed a small local conformational change close to the C-terminus induced by the cognate ligand binding (*1*, *5*). The activated PBP (LUSH from *Drosophila*) can itself activate olfactory sensilla, presumably through the odorant receptor (OR) (*5*).

PBPs have also been suggested to be a carrier that transports the ligand through the lymph to the OR and may also protect the ligand from the degrading enzymes that are secreted into the lymph (*6*). PBPs are also suggested to be a scavenger that protects the neurons at high ligand concentration (*7*). A good way to study the function is to investigate the interactions between a ligand and the PBP, such as the binding affinities represented by the dissociation constants, or molecular recognition represented in the crystal structure. More pieces of information about this protein family have been brought together gradually. From the study of binding affinities, we know that PBPs are capable of binding a variety of ligands selectively, but this selectivity does not correlate with the selectivity observed in the insect olfactory system (*7*). In the available 3D structures of PBPs bound with a ligand, it appears that the binding pockets of the PBPs are flexible and can accommodate ligands of various volumes. For example, BmorPBP from silk moth (*8*, *9*), ASP1 from honey bee (*1*), LUSH from *Drosophila* (*5*, *10*), and LamPBP from cockroach (*11*) have been crystallized with both pheromonal and nonpheromonal ligands.

Our group is interested in the dynamics of PBP−ligand interactions in solution. We have proposed previously a two-step association mechanism based on kinetic studies with PBP2 (Figure 1) (*12*). We suggested that a ligand will associate with the protein on an external site before entering the internal binding pocket. In other words, there are two binding states of a ligand on the protein, externally bound ($P \cdot L_{ext}$) and internally bound ($P \cdot L_{int}$). A hydrophobic patch on the protein surface could be

†This work is funded by the Natural Sciences and Engineering Research Council of Canada (NSERC) for E.P., NSERC Strategic (STGRP307515) and NSERC Discovery (RGPIN222923), and for C.B., NSERC Discovery (RGPIN121389).

*To whom correspondence should be addressed. E-mail: plettner@sfu.ca. Tel: (778) 782-3586. Fax: (778) 782-3765.

[1]Abbreviations: aa, amino acids; ANS, 8-anilinonaphthalene-1-sulfonic acid; CD, circular dichroism; GC-MS, gas chromatography−mass spectroscopy; NPN, *N*-phenyl-1-naphthylamine; OR, odorant receptor; PBP, pheromone-binding protein; TPBP, C-terminally truncated PBP; (+)-disparlure, 2-methyl-7(*R*),8(*S*)-epoxyoctadecane.


Published on Web 12/17/2009

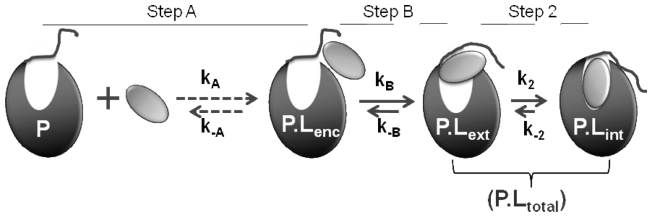


FIGURE 1: Illustration of stepwise association of a ligand with PBP. This is the expanded model based on the previous model (solid arrows) (*12*). The ligand (ellipse) first collides with the protein in a diffusion-controlled step (dashed arrows, from this work), forming an encounter complex, $P \cdot L_{enc}$, which may decay to a relatively stable complex, $P \cdot L_{ext}$. The C-terminal peptide (random coil) of the PBP may be involved. In the last step, the ligand is slowly internalized. In the previous study, the first two steps were unresolved. In this work, we have followed the formation of $P \cdot L_{total}$.

a potential external binding site, and we have suggested a region composed of the loop connecting helices 2 and 3 and the C-terminal segment for this site. Because of the limitations of the technique we have used before, a different method was needed to study the external binding process as well as the kinetics of PBP1. In this paper, we have used a fluorescent compound, *N*-phenyl-1-naphthylamine (NPN), as a surrogate to study the ligand interaction kinetics of both PBP1 and PBP2 and their truncated forms which are lacking the C-terminal segment, TPBP1 and TPBP2. NPN is a very good fluorescent reporter. When present in a hydrophobic environment, its fluorescence increases dramatically, compared to its fluorescence in an aqueous environment. A similar compound, 8-anilinonaphthalene-1-sulfonic acid (ANS), has been crystallized in the internal cavity of LmaPBP (*11*). We believe that the NPN can also enter the binding pocket of PBP and the study of NPN−PBP interaction kinetics can provide us with more insight into the dynamics of PBPs in solution.

In this work, we present stopped-flow kinetic data for the two PBPs and TPBPs with NPN. The results support stepwise binding. In addition to the two binding states of the protein−ligand complex we suggested before ($P \cdot L_{ext}$ and $P \cdot L_{int}$), there is another binding state where the ligand is bound peripherally ($P \cdot L_{enc}$). By comparing the truncated and the full-length PBPs, we suggest that the C-terminal peptide of the long-chain PBPs may assist ligand binding. In addition, we have monitored the conformational changes in these proteins, by monitoring quenching of the tryptophan fluorescence, in the presence of the pheromone of the gypsy moth ((+)-disparlure) or of NPN. Our results suggest that the pheromone ligand induces a different local conformation around Trp 37 from what is induced by the nonnatural ligand. We have attempted to correlate the time regime of the conformational changes to that of certain kinetic steps. A hypothesis is that each kinetic step may confer different functions to the PBPs. In other words, different $P \cdot L$ states may serve different functions.

## EXPERIMENTAL PROCEDURES

*Protein Production and CD Spectra*. Recombinant PBPs were expressed and purified as previously described (*13*). The C-terminally truncated PBPs (TPBPs) were constructed by a PCR-based approach to delete the C-terminal fragment from Trp 129 to Gln 145 for TPBP2 and from Trp 128 to Thr 143 for TPBP1 (*12*).

CD spectra of PBPs and TPBPs in 20 mM Tris buffer, pH 7.4, at protein concentration 10 $\mu$M were acquired on a JASCO J-810 spectropolarimeter equipped with a Peltier type PFD-425S constant temperature cell holder. Far-UV measurements were made between 190 and 260 nm at 25 °C using a quartz cell with 0.1 cm light path length. Data were recorded using three accumulations, each at a scan rate of 200 nm/min, with a response time of 0.1 s. A baseline was subtracted from all spectra. Secondary structure contents of each protein were determined by the CDPro program (http://lamar.colostate.edu/~sreeram/CDPro/main.html) using two methods: SELCON3 and CONTINLL. Two sets of reference proteins were used for secondary structure calculation: 43 proteins and 56 proteins. The average values from four quantities (two methods and two reference sets) are presented.

*Different Binding Affinities between Proteins*. The dissociation constants of PBP−NPN complexes were obtained with two methods. First, a separation of the unbound NPN from the protein-bound NPN by a size exclusion minicolumn was followed by GC-MS-based quantification of the NPN amount. This is a slightly modified procedure from previous ones (*12*, *13*). Tests were done at room temperature for equilibrated 4 $\mu$M protein and 8 $\mu$M NPN in 20 mM Tris buffer, pH 7.4. A minicolumn filled with Sephadex G-10 powder (instead of the P-2 gel, Bio-Rad, we have used previously) was used to remove the free NPN for each sample. Four replicates were conducted for each condition.

A second method was based on the increase in the NPN fluorescence when the NPN molecule is located in a hydrophobic environment. A series of NPN/MeOH stock solutions were prediluted from 2 mM stock to final concentrations of 0, 0.1, 0.2, 0.3, 0.6, 0.9, 1.2, and 1.5 mM. We then added 2 $\mu$L of the prediluted solutions to 200 $\mu$L of 4 $\mu$M PBP solutions in corresponding wells on the 96-well plate. Protein solutions were prepared in 50 mM phosphate buffer, pH 7.0. There were three replicates for each protein. Controls in the phosphate buffer without PBPs were conducted on the same plate. Plates were then scanned at 385 nm with Cary Eclipse fluorometer when excited at 337 nm. Each plate was scanned after 1 h incubation.

*Stopped-Flow Kinetics for PBP−NPN Association*. NPN is a good fluorescence reporter for ligand binding. It dissolves well in aqueous buffer up to 30 $\mu$M (Supporting Information Figure S1) and fluoresces stably and significantly in protein solutions (Supporting Information Figure S2). A SX20 stopped-flow system from Applied Photophysics Ltd. was employed to measure the kinetics of NPN binding with PBPs. The excitation wavelength was adjusted to 337 nm by an excitation monochromator with a slit width corresponding to a bandwidth of 2 nm. The fluorescence emission was collected at 396 nm which was set by an emission monochromator with a bandwidth of 8 nm. Protein solutions (1, 1.5, 2, 2.5, and 3 $\mu$M) and NPN solutions (0.25 $\mu$M) were prepared by dissolving the appropriate amounts of protein and NPN stock solutions into 20 mM Tris buffer, pH 7.4, respectively. The protein solution was contained in one syringe while the NPN solution was contained in the second syringe, and the two solutions were mixed in a 1:1 ratio. Therefore, the final concentrations of NPN and protein are half of the concentrations stated above. Samples were thermostated at 20.0 ± 0.1 °C for at least 15 min using a circulating water bath before experiments were performed.

The kinetic data were collected for 0.2 or 0.5 s, and the mixing time was 1 ms. For each experiment 20 individual traces were averaged. To evaluate the rate constants, the averaged kinetic traces were analyzed using the Pro-Kineticist II software from

Applied Photophysics. As a test, the data were fit with different functions, such as monoexponential and the sum of two exponential functions (see Supporting Information for details on other fits tried). At the end, global fits were employed to analyze all of the kinetic traces. Global fits simultaneously fit all of the kinetic traces for each protein at different conditions (in our case, different protein concentrations) to reactions A and B.

$$P + L \underset{k_{-A}}{\overset{k_A}{\rightleftharpoons}} P\cdot L_{enc} \quad (A)$$

$$P\cdot L_{enc} \underset{k_{-B}}{\overset{k_B}{\rightleftharpoons}} P\cdot L_{total} \quad (B)$$

Similarly, in a second experiment, 0.25 $\mu$M PBP1 was studied for its binding with NPN at various concentrations (0.005, 0.05, 0.125, 0.25, 0.5, 1.25, 2.5, and 5 $\mu$M). The averaged kinetic traces were used to get the initial rates of the association at each NPN concentration. To estimate the initial rate of association, slopes for each kinetic trace were obtained from the first derivative near ~2 ms, which corresponds to the time after mixing in the stopped-flow system, and those values were used as the initial rate in plots of initial rate against NPN concentration.

*Fluorescence Quenching Studies*. (*A*) *Ratio of the Quenching Constants Is an Indicator of the Local Environment*. Quenching of fluorescence can be used to measure the accessibility of a quencher to a fluorophore. We used a neutral quencher, acrylamide, and an anionic quencher, iodide, to determine if these quenchers had differential accessibility to Trp residues in the PBPs and TPBPs.

Fluorescence quenching is measured as a decrease of the fluorescence intensity in the presence of quencher ($F$) when compared to the intensity in the absence of quencher ($F_0$), where a linear relationship with the quencher concentration is expected (eq 1, Figure 4) (*19*).

$$\frac{F_0}{F} = 1 + K_{SV}[Q] \quad (1)$$

$K_{SV}$ is defined as the Stern−Volmer constant which carries the unit of $M^{-1}$, and its value is equal to the product of the quenching rate constant ($k_q$, $M^{-1}$ $s^{-1}$) and the lifetime of the fluorophore, in this case Trp, in the absence of quencher ($\tau_0$, s) ($K_{SV} = k_q\tau_0$). The accessibility of the quencher to the fluorophore is related to the values of $k_q$. Studies showed that the lifetime of Trp varied when ligands were bound (unpublished results), and therefore, the Stern−Volmer constants cannot be directly related to the accessibility of the quenchers. However, for each ligand the ratio of the Stern−Volmer constant for acrylamide ($K_{SV}^{Acr}$) and iodide anions ($K_{SV}^{I}$) is equal to the ratio of the $k_q$ values (eq 2). A change in this ratio indicates that the environment around Trp is different, and it changes either the accessibility of the neutral quencher or the ionic quencher or both.

$$\frac{K_{SV}^{Acr}}{K_{SV}^{I}} = \frac{k_q^{Acr}\tau_0^x}{k_q^{I}\tau_0^x} = \frac{k_q^{Acr}}{k_q^{I}} \quad (2)$$

(*B*) *Procedure*. Portions of 5 mM quencher (potassium iodide or acrylamide) stock solutions were added consecutively to 500 $\mu$L of 2 $\mu$M protein samples either without or with ligand. To estimate the exposure of the Trp residue in the PBP−ligand complex, 10 $\mu$M (+)-disparlure was used for all of the proteins and 8 and 40 $\mu$M NPN was used for PBP1/TPBP1 and PBP2/TPBP2, respectively. The high concentration of NPN used for PBP2 and TPBP2 ensured a good percentage of PBP−NPN complexes. The PBP and ligand mixtures were incubated for at least 2 h before each test. Three independent samples under each condition were used. For the short-time incubated PBP2−(+)-disparlure sample, ligand stock was added to the protein solution with the desired quencher concentration. The mixture was quickly shaken and scanned within 25 s. Each point represents the average of three replicates. Samples were excited at 295 nm, and data were collected from 310 to 350 nm on a PTI fluorometer equipped with an 814 photomultiplier detection system at 20 °C.

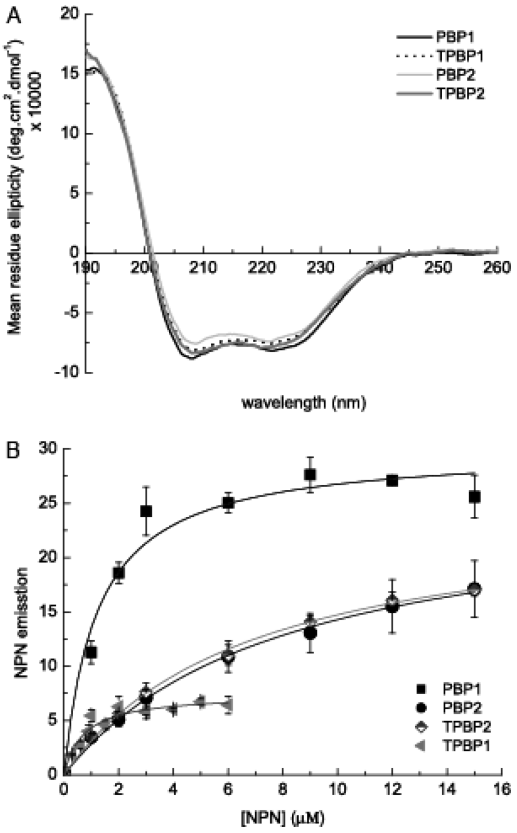


FIGURE 2: Difference in the secondary structure (A) and the binding affinity with NPN (B) between PBP1, TPBP1, PBP2, and TPBP2. (A) Far-UV CD spectra of 10 $\mu$M proteins. (B) Binding of NPN to PBPs/TPBPs indicated by the fluorescence increase. Bars indicate standard error of three replicates.

## RESULTS

*Truncation Has Little Effect on PBP Core Structure*. Figure 2A shows the far-UV CD spectra of PBP1, TPBP1, PBP2, and TPBP2. The shapes of the spectra are characteristic of proteins with a high percentage of helical structure. The spectrum of TPBPs overlaps very well with that of the corresponding PBPs in both the shape and the amplitude, except that there is an ~8% decrease in the amplitude of the negative 222 and 208 nm bands for TPBP1 and ~7% and 11% increases for each band, respectively, for TPBP2. The secondary structure fractions calculated from CD spectra in Figure 2A are listed in Table 1. The average values from four calculations and the standard deviations between calculations are presented for each type of secondary structure. Overall, consistent with the reported structures of PBPs from other insects (*9*−*11*, *14*−*16*), all of the proteins tested here contain more than 90% helical structures. The truncation did not affect the protein structures on the secondary level, and based on

Table 1: Secondary Structure Components of PBPs/TPBPs from the Analysis of CD Spectra in Figure 2A with the CDPro Program[a]

| protein | H(r) | H(d) | S(r) | S(d) | T | unrd |
|---|---|---|---|---|---|---|
| PBP1 | 71 ± 4 | 25.1 ± 0.7 | 0 | 0.1 ± 0.9 | 3 ± 2 | 7 ± 5 |
| PBP2 | 74 ± 6 | 21 ± 4 | 0 | 0.6 ± 0.2 | 4 ± 3 | 10 ± 6 |
| TPBP1 | 70 ± 4 | 23.9 ± 0.9 | 0 | 0.8 ± 0.5 | 4 ± 3 | 9 ± 6 |
| TPBP2 | 79 ± 9 | 16 ± 6 | 0 | 0.3 ± 0.4 | 4 ± 3 | 8 ± 5 |

[a]Numbers indicate the percentage of each component. Two methods and two sets of reference proteins are used (±SE). Abbreviations: H, helices; S, strands; T, turns; unrd, unordered; r, regular; d, distorted.

Table 2: Dissociation Constants of PBPs/TPBPs with NPN ($K_d$ in $\mu$M)[a]

| protein | GC | fluorescence |
|---|---|---|
| PBP1 | 7 ± 4 | 1.3 ± 0.3 |
| PBP2 | 66 ± 8 | 8.6 ± 0.6 |
| TPBP1 | 6 ± 2 | 1.0 ± 0.2 |
| TPBP2 | 300 ± 164 | 7.7 ± 0.8 |

[a]For the GC results, data are reported as the average of four replicates ± SE; for the fluorescence results, data are obtained from the one-site binding model fit of curves in Figure 2B; errors represent the fitting error.

the high resemblance of the CD spectra, we assume that the tertiary core structures of PBP1 and PBP2 are preserved in their truncated forms.

We also notice that the pair of PBP2 and TPBP2 has a slightly higher content of regular helix than the pair of PBP1 and TPBP1. The tertiary structure predicted by the CLUSTER program (*17*) for the first pair of proteins is in the all-α class, and for the latter one, it is in the $\alpha + \beta$ class. The difference may also be represented by a slight difference in the shape of the 190 nm band, and the shape of the specific band for PBP2/TPBP2 is similar to the reported one for BmorPBP (*4*). Unfortunately, there are no crystal structures available for PBP1 and PBP2 yet. PBP1 and PBP2 share 55% similarity in the amino acid sequence. We expect a subtle but possibly important difference between their structures based on the limited information provided by the CD spectra on the secondary structure.

*Different Binding Affinities of the Proteins for NPN*. The binding affinities of PBPs with NPN have been evaluated by two methods: first, the GC technique, and second, fluorescence titration (Figure 2B). Different $K_d$ values were obtained from each method. However, consistently, the binding affinities from the strongest to the weakest were PBP1 ≈ TPBP1 > PBP2 ≥ TPBP2 (Table 2). Consistent with previous observations, losing the C-terminal peptide has weakened the binding affinity of PBP2 in the GC assay (*12*) but not in the fluorescence assay. Interestingly, the binding affinity of PBP1 is not affected by the truncation, as detected with either method.

The $K_d$ values from the fluorescence assay were overall smaller than those from the GC assay. Especially for TPBP2, two $K_d$s differ by a factor of 40. Both the GC and fluorescence assays were done at 4 $\mu$M PBP concentration, and the same range of NPN concentration was used, so this should not be a result of binding enhancement induced by PBP multimerization at high ligand:protein ratio (*7*). From the analysis of the stopped-flow data in Table 3 for PBP1, where $k_B/k_{-B} > 10$, the concentration of $P \cdot L_{total}$ is much larger than that of $P \cdot L_{enc}$. This might be true for the other three PBPs as well. Therefore, the existence of the $P \cdot L_{enc}$ could not be the reason for the difference in $K_d$ between two assays.

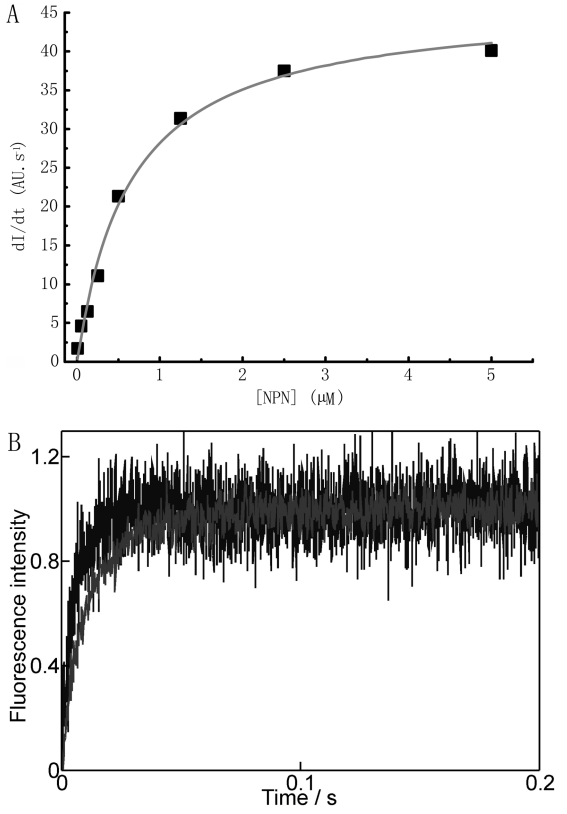


FIGURE 3: (A) The initial rate of PBP1 binding with NPN is saturable at high NPN concentration. Various NPN concentrations (0.005−5 $\mu$M) were used for binding with 0.25 $\mu$M PBP1. The initial rate was the maximal value, nearest to 2 ms, of the first derivative of the corresponding kinetic trace, such as those shown in panel B. (B) Normalized kinetic trace for 1.5 $\mu$M protein binding with 0.125 $\mu$M NPN (gray, PBP1; black, TPBP1).

*Stopped-Flow Kinetics Revealed Two-Step Binding of NPN to PBP*. Two observations suggest that NPN follows a two-step binding process to PBPs. First, the kinetic traces of PBP1 cannot be fit to a monoexponential function (Supporting Information Figure S3A), indicating that there was more than one kinetic process; reactions A and B were considered for the fit of the kinetic data acquired for PBP1. Second, the initial rate of binding is saturable (Figure 3A), and this indicates that a quickly built equilibrium (step A) leads to the formation of the bound complex (step B). These two reactions correspond to a model where an encounter complex is formed in a bimolecular reaction followed by the unimolecular relocation of the ligand. However, in the stopped-flow experiment for PBP1 the kinetic data were fit to a sum of two exponentials, whereby each exponential term corresponds to one relaxation process. The first relaxation process is fast and close to the time resolution of the experiment. For this reason, a series of global fits were performed in which the values for $k_A$ were fixed to incremental values between $1 \times 10^9$ $M^{-1}$ $s^{-1}$ and $1 \times 10^6$ $M^{-1}$ $s^{-1}$. Random residuals and similar standard deviations were observed for $k_A$ values between $1 \times 10^8$ $M^{-1}$ $s^{-1}$ and $4 \times 10^7$ $M^{-1}$ $s^{-1}$ (Table 3). These led to an upper limit for $k_{-A}$ of 25 $s^{-1}$. Reaction B corresponds to a unimolecular relaxation process. The observed rate constant for this process ($k_{obs,B}$) is equal to the sum of $k_B$ and $k_{-B}$. In the case of PBP1, the fits converged to a value of 0 for $k_{-B}$. Simulations of the kinetics indicated that a value of $k_{-B}$ corresponding to 10% of $k_B$ would be discernible for the signal-to-noise ratio of the

Table 3: Kinetic Parameters for the Interaction between PBPs/TPBPs and NPN

| protein | $k_A$ ($\times 10^7$ $M^{-1}$ $s^{-1}$) | $k_{-A}$ ($s^{-1}$) | $k_{obs,B}$ ($s^{-1}$) |
|---|---|---|---|
| PBP1 | 4−10[a] | <25 | 61 ± 9[b,c] |
| PBP2 | nd | nd | 56 ± 4[c] |
| TPBP1 | nd | nd | 168 ± 3[c] |
| TPBP2 | nd | nd[d] | 133 ± 8[c] |

[a]Values for $k_A$ were fixed, and for the range of $k_A$ values stated, random residuals were observed for the fit and experimental data. [b]This value corresponds to $k_B$, and $k_{-B}$ was estimated to be smaller than 6 $s^{-1}$. [c]Errors correspond to the errors recovered from the global fit analysis of the Pro-Kineticist II software from Applied Photophysics. [d]nd = not detected. The formation of $P\cdot L_{enc}$ was faster than the time resolution of the stopped-flow instrument but must have taken place because $k_{obs,B}$ was independent of protein concentration (see text).

kinetic measurements with PBP1 (see details in the Supporting Information). These simulations led to an upper limit of 6 $s^{-1}$ for $k_{-B}$.

The second result that supports the two-step binding process for PBP1 is that its initial rate of association with NPN is saturable at high NPN concentration (Figure 3A). The saturability of the initial association rate is consistent with the existence of an intermediate ($P\cdot L_{enc}$). Fitting of the data to the Michaelis−Menten equation gives a $K_m$ value of 0.64 ± 0.07 $\mu$M.

In the case of PBP2, TPBP1, and TPBP2, the kinetic data can be fit to both a monoexponential function and the sum of two exponentials (for example, Supporting Information Figure S3B for TPBP1). For these three proteins the kinetic data were fit to a monoexponential function (Supporting Information Figures S3 and S4). The observed rate constant, $k_{obs,B}$, for PBP2, TPBP1, and TPBP2 did not depend on the protein concentration, and therefore the kinetics corresponds to the unimolecular step of reaction B, whereas reaction A occurs on a time scale faster than the time resolution of the stopped-flow instrument (1 ms). Only $k_{obs,B}$ could be determined. However, the similarity between the $k_B$ value for PBP1 and $k_{obs,B}$ for PBP2 suggests that the major contribution to the observed rate constant was probably from $k_B$ for the two proteins.

A qualitative comparison of the kinetics for PBP1 and TPBP1 shows that equilibration is faster for TPBP1 than for PBP1 (Figure 3B). For PBP1 the formation of $P\cdot L_{enc}$ is slow enough to be observed on the time scale for stopped-flow experiments. The time constant for the generation of $P\cdot L_{enc}$ is equal to the sum of the association and dissociation processes ($k_A$[protein] + $k_{-A}$). For the other three proteins the kinetics was adequately fit to a monoexponential function, and the kinetics was not dependent on the protein concentration, indicating that the formation of $P\cdot L_{enc}$ occurred with a time constant higher than $10^3$ $s^{-1}$. Since the $k_A$ value for PBP1 is close to a diffusion-controlled ligand−protein encounter (normally ~$10^7$ $M^{-1}$ $s^{-1}$) (*18*), the higher time constant for the other three proteins is dictated by a much higher value for $k_{-A}$, i.e., the dissociation of $P\cdot L_{enc}$. The second process, which is related to the incorporation of the ligand into the protein, was shown to be similar for PBP1 and PBP2 or TPBP1 and TPBP2, where higher values for $k_{obs,B}$ were observed for the latter two proteins.

The disadvantage of using NPN to study the PBP−ligand interaction kinetics is that NPN is nonnatural, but nevertheless, the results provide us with three new insights (Table 3).

First, the results for PBP1 indicate the existence of a unimolecular step. These results support and further expand our model that a ligand, whether natural (*12*) or not (NPN), is introduced into the protein binding pocket in a stepwise manner. Although the kinetics for PBP2, TPBP1, and TPBP2 do not directly reveal the fast first binding step, such a process to generate $P\cdot L_{enc}$ must occur because the observed relaxation kinetics did not show a dependence on the protein concentration, indicating that it corresponded to a unimolecular reaction.

Second, PBP1 and PBP2 show different binding modes at the initial encounter, with a faster process being observed for PBP2. Since PBP1 and PBP2 should have $k_A$ values in the same magnitude (diffusion-controlled step), the faster relaxation process for PBP2 is due to a higher $k_{-A}$ leading to a higher $K_d$ value for the formation of $P\cdot L_{enc}$ in the case of PBP2. Although PBP1 and PBP2 have similar $k_B$ values, the larger $k_{-A}$ value for PBP2, which competes with the forward reaction, led to an overall slower reaction rate for PBP2.

Third, loss of the C-terminal peptide leads to a faster relaxation process for the relocation of the nonnatural ligand, NPN. The values of $k_{obs,B}$ correspond to the sum of the relocation of the ligand into the protein and dissociation of the ligand back to the first encounter complex, and one or both of these rate constants increased with the removal of the C-terminal peptide when compared to the PBPs. This result supports the idea that the C-terminal peptides of long-chain PBPs are gating the binding pocket.

*Local Conformational Changes around Trp 37 upon Ligand Binding Detected by Tryptophan Fluorescence Quenching Studies*. In order to understand the meaning of the ratio better, we have to realize that there is a difference between the intrinsic capabilities of acrylamide and iodide to quench the excited indole ring. Acrylamide has been indicated as an effective and potent quencher for tryptophan fluorescence through collisional processes (*20*). Its quenching efficiency is mostly affected by the steric hindrance around the Trp residue. The highly hydrated and charged iodide ion does not quench the tryptophan fluorescence as effectively as acrylamide. Under our test conditions (pH 7.4, 20 mM Tris buffer), the $K_{SV}$ constants for iodide and acrylamide to quench the free tryptophan are 8.6 $M^{-1}$ and 18.1 $M^{-1}$, respectively, giving a ratio of 2.1 ± 0.2 (Supporting Information Table S1). Moreover, the electronic environment around a tryptophan residue also affects the quenching efficiency of iodide. A positively charged environment around Trp can increase significantly the quenching degree by an anionic quencher (*21*). Therefore, the ratio of the Stern−Volmer constants represents the overall environment around the tryptophan residue (Trp 37 in our case; see below), including the steric and electronic factors.

If the Trp residue in a protein is exposed to the solvent and not in the vicinity of any charged residues, it should have a ratio of Stern−Volmer constants for the two quenchers close to the ratio observed for free Trp. A larger ratio indicates a more negative environment around Trp (smaller $K_{SV}^{I}$), and a smaller ratio may imply either a more positive (larger $K_{SV}^{I}$) or a more sterically hindered (smaller $K_{SV}^{Acr}$) environment around Trp. Thus, larger ratios observed for apo-PBP1 and apo-PBP2 have indicated that Trp 37 in both proteins is solvent-exposed and in the proximity of some negative residues (Table 4).

(*A*) *Trp 37 Was the Residue Monitored*. There are two conserved tryptophan residues in LdisPBPs, Trp 37 and 129. The first one is on the α2/3 loop, and the second one is on the C-terminal peptide and connects the C-terminus to the sixth helix of the protein, as predicted from the threaded structures

of these proteins (*12*). It is eliminated in both TPBP1 and TPBP2.

The reasons why we mostly refer to Trp 37 in our discussion and interpretation of the results about the environment of tryptophan residue(s) in the proteins are as follows. First, previous studies have shown that Trp 129 in two other moth PBPs does not contribute significantly to the protein tryptophan fluorescence (*22*, *23*). In our case, the Trp fluorescence intensity of TPBPs was weaker than that of the full-length PBPs (Supporting Information Figure S5). This was expected because losing the C-terminal peptide can potentially make the nearby Trp 37 more exposed. Second, multi-tryptophan proteins have been loosely categorized into three groups based on the curvature of their Stern−Volmer plots: (1) upward curving, all residues nearly equally accessible or one single residue dominating; (2) downward curving, heterogeneous fluorescence residues having a widely different accessibility to quencher; (3) linear plot, heterogeneous fluorescence residues differing slightly in accessibility (*20*). We have carefully examined all of our plots, and none of them falls into the second category (Figure 4). This means either the fluorescence is dominated by Trp 37 or both tryptophan residues have similar accessibility. The first one is a more likely scenario. Third, TPBPs only have one tryptophan (Trp 37). Therefore, we would expect that any decrease in Trp fluorescence from quenching should primarily come from Trp 37 in those proteins.

(*B*) *Local Conformational Changes Induced by Ligands*. For all of the proteins the ratio of the Stern−Volmer constants decreased when ligands were bound, suggesting a change in the environment around Trp 37 leading to either a decrease in the acrylamide accessibility or an increase in the accessibility of the negative iodide anion. Trp 37 is predicted to be on the α2/α3 loop of the protein. This change is ligand-specific for both PBPs between (+)-disparlure, (−)-disparlure, and NPN ligands and is not directly related to the binding constant of the ligand. For example, PBP1 and (+)-disparlure have a $K_d$ value of 7.1 μM (*13*) and a ratio of 1.3. PBP1 and NPN also have a $K_d$ of 7 μM but a ratio of 0.9. Similarly, TPBP1 and NPN have a $K_d$ of 6 μM and a much smaller ratio of 0.38 (Tables 2 and 4). Interaction with different ligands results in subtly different conformations of the protein. Another consistent observation is that PBP1 and PBP2 had different pH profiles with (+)- and (−)-disparlure (*24*), suggesting that different ionizable groups are exposed with different ligands.

Since we have reported a slow process for PBP2 and (+)-disparlure interaction (in seconds) (*12*), we were curious whether the ligand-specific local environmental change we observed here is associated with that process. We obtained the ratios for PBP1 and PBP2 in different complexes at short incubation lengths (< 25 s). The results have shown that the ratio decreases immediately after the protein and ligand are mixed to the same level of the extensively incubated mixture (Figure 5).

(*C*) *Truncation of the C-Termini Had Different Effects on PBP1 and PBP2*. Overall, TPBPs have smaller ratios of the

Table 4: Ratio of the Stern−Volmer Constants for the Quenching of the Fluorescence of Trp by Acrylamide ($K_{SV}^{Acr}$) and Iodide Anions ($K_{SV}^{I}$)[a]

| | ligand | | | |
|---|---|---|---|---|
| protein | none | (+)-disp | (−)-disp | NPN |
| PBP1 | 2.4 ± 0.2 | 1.3 ± 0.1 | 1.0 ± 0.1 | 0.9 ± 0.1 |
| PBP2 | 2.9 ± 0.2 | 1.1 ± 0.1 | 0.76 ± 0.08 | 1.6 ± 0.2 |
| TPBP1 | 1.6 ± 0.2 | 0.81 ± 0.07 | 0.34 ± 0.02 | 0.38 ± 0.04 |
| TPBP2 | 1.9 ± 0.2 | 1.14 ± 0.06 | 0.76 ± 0.05 | 1.2 ± 0.1 |

[a]Data were obtained for apo-PBPs/TPBPs and protein complexes with different ligands. The $K_{SV}$ values are shown in Supporting Information Table S2, and the errors correspond to the error propagation from the errors for the individual $K_{SV}$ values.

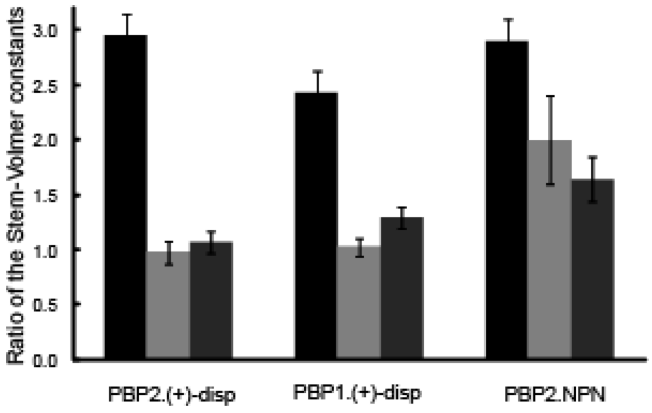


FIGURE 5: Ratio of the Stern−Volmer constants of intrinsic Trp in apo-PBP (black), the PBP−ligand complex with short incubation (gray), and PBP−ligand complexes with long incubation (dark gray). Bars indicate the error propagation from the errors for the individual $K_{SV}$ values.

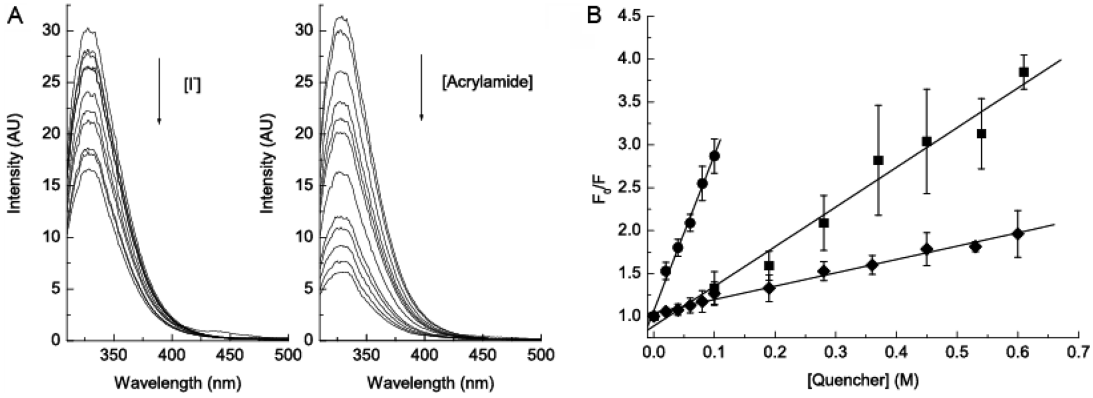


FIGURE 4: Examples of fluorescence quenching. (A) Spectra of intrinsic tryptophan fluorescence of apo-PBP2 at different quencher concentrations. $\lambda_{ex}$ = 295 nm. (B) Stern−Volmer plots for apo-PBP2 and free tryptophan (diamonds, PBP2 quenched by iodide; squares, PBP2 quenched by acrylamide; circles, free tryptophan quenched by acrylamide; bars indicate standard error for three replicates).

Stern−Volmer constants than PBPs. This might be a direct result of the elimination of the negative residues on the C-terminal peptide. On the basis of the results from the quenching study, we concluded that the C-terminal peptide may play different roles in different LdisPBPs. For example, binding of (+)-disparlure with TPBP2 induced a smaller decrease in the ratio (40%) than with PBP2 (62%). TPBP1 and PBP1 had comparable decreases in the ratio for binding with (+)-disparlure (49% and 46%, respectively) (Table 4). Losing the C-terminus seemed to have a larger effect on PBP2.

## DISCUSSION

*Stepwise Association of a Ligand on the PBP*. We proposed a two-step binding mechanism for the association of PBP2 with (+)-disparlure and with (−)-disparlure (*12*): a ligand is bound externally before it is docked into the internal binding pocket (Figure 1).

This study has provided further evidence for a stepwise binding mechanism. First, the traces of stopped-flow fluorescence for the association of PBP1 with NPN fit best to a model of two sequential reactions (Supporting Information Figure S3). The first one is a diffusion-controlled bimolecular reaction, and the second one is a unimolecular reaction (Table 3). Second, the initial association rate of PBP1 binding with NPN is saturable at high NPN concentration, and the kinetics for the other proteins is unimolecular. This suggests the formation of a $P \cdot L$ intermediate before the final product and, therefore, indicates a two-step binding model. It is reasonable to propose that the two molecules need to collide before they associate. Therefore, we can conclude that LdisPBPs and their truncated forms first associate with the ligand through diffusion-controlled collision, forming the encounter species $P \cdot L_{enc}$. From $P \cdot L_{enc}$, the ligand is then relocated to a different site or binding mode. This should be generally true for the other PBPs.

However, when compared with previous results, we also noticed that binding of PBP2 with NPN is much faster than with disparlure. The latter has a $k_2$ value in the magnitude of $10^{-4}$ $s^{-1}$ whereas $k_B$ (the rate constant for reaction B) for PBP1−NPN binding is 61 $s^{-1}$. Reasons causing this discrepancy could be (1) different techniques used, (2) different ligands tested, or (3) different processes followed. We believe that the $k_2$ value we have measured before describes a different process from reaction B here for three reasons, but before describing these, we have to clarify the notation "external binding site" we used before.

In the previous work, we found that the mixing of dansylated PBP2 with (+)-disparlure led to an immediate loss in the dansyl fluorescence intensity (≤5 s), followed by a slow decrease of the fluorescence. The first decrease was attributed to a rapid interaction between the protein and the ligand, and we suggested an external binding site for that interaction (*12*). The exact position of the external binding site was unknown, and the word "external" was used to distinguish it from the internal binding site that binds ligand stably. It may be more suitable to call them different binding "modes" of the ligand instead of "sites" to eliminate possible confusion.

We believe that the previously reported $k_2$ value describes a different process than $k_B$ reported here, for three reasons. First, different binding modes of the ligands in the binding cavity of OBPs have been observed. For example, bombykol in each BmorPBP monomer (*9*) and *cis*-vaccenyl acetate in each LUSH monomer (*5*) in the dimeric crystal structures have different ligand and protein conformers. In addition, there are different binding domains in the binding pocket. Two bell pepper molecules were modeled in the BmorPBP binding pocket (*8*), and a plastic compound (*n*-butyl benzenesulfonamide) was modeled in a different domain from the queen pheromone molecule (9-keto-2(*E*)-decenoic acid) in the ASP1 binding cavity (*1*).

Second, a three-step binding model has been proposed for other proteins, cytochrome P450 3A4, for example (*25*). The ligand bound at a peripheral site in the initial rapid encounter (step 1) translocates to the active binding pocket (step 2) and then induces a conformational change of the protein (step 3). There may be a similar situation for PBPs. We may have followed the global protein conformational changes induced by the ligand instead of the relocation of the ligand into the binding pocket in the previous paper by following the fluorescence decrease of the covalently attached dansyl group. In this paper, by following the ligand (NPN) fluorescence change, we have monitored the binding process from the ligand's aspect. We have isolated the rapid, real external binding of the ligand, but we may not be able to tell apart the two binding modes of the ligand in the pocket, namely, $P \cdot L_{ext}$ and $P \cdot L_{int}$ (Figure 1).

Third, the small amount of the $P \cdot L_{enc}$ is not sufficient to account for the difference in $K_d$ values between GC and fluorescence assays. We hypothesize that there are two binding modes of the ligand in the protein: $P \cdot L_{ext}$ and $P \cdot L_{int}$. The latter is more stable than the former and also the encounter complex $P \cdot L_{enc}$. All three species fluoresce. Therefore, there are two possibilities for the differences between the $K_d$ values by GC and fluorescence experiments: (i) GC measures $P \cdot L_{int}$ but not $P \cdot L_{enc}$ and $P \cdot L_{ext}$, and fluorescence measures all three, or (ii) GC measures $P \cdot L_{int} + P \cdot L_{ext}$ but not $P \cdot L_{enc}$, and fluorescence measures all three species. The former might be more plausible considering that the concentration of $P \cdot L_{enc}$ is low.

Overall, we suggest a third step following the two relaxation processes observed in this work, the conversion of the bound ligand from the less stable to the more stable binding mode. This step is characterized by the parameters $k_2$ and $k_{-2}$. For the interaction between PBP2 and (+)-disparlure, the $k_2$ value is 4.3 $\times$ $10^{-4}$ $s^{-1}$ (*12*). The parameter $k_1$ in the previous work is most likely a composite of processes A and B from this work.

*Ligand Discrimination by PBP1 and PBP2*. Our group has compared these two proteins for years with regard to the binding properties and structures (*7*, *13*, *24*, *26*). PBP1 and PBP2 differ significantly in primary sequence, binding affinities with structurally related ligands (*7*, *13*, *27*), and pH profiles of ligand binding (*24*). However, in terms of overall structure, the proteins are very similar (ref *26* and Figure 2A). We are curious about the reason why the moth produces two PBPs and wish to explore the possible connections between the PBP binding and the selectivity in the pheromone sensing of insects. It is reported that PBPs are capable of binding many different compounds, natural or unnatural (*1*, *8*−*11*, *28*). We have found that the dissociation constants of various compounds are not directly related to their biological function (unpublished data and ref *7*). Two explanations are possible: either PBPs do not discriminate and the selectivity of the olfactory system only comes from the downstream component such as the odorant receptors, or PBPs discriminate ligand in a subtle but elegant way.

Recent literature has drawn our attention to the importance of the C-terminal peptide of PBPs and the local conformational change of PBPs induced by a biofunctional ligand (*1*, *5*).

This suggests that PBPs contribute to ligand discrimination through their elaborate conformational changes, seen only with biologically relevant ligands. We have probed this kind of conformational change before by testing the pH profiles of PBP1 and PBP2 with different ligands (*24*). The pH profile indicates the environment of the residues being titrated and therefore reflects indirectly the local conformational changes in each case.

In this study, we have shown different local conformational changes induced by ligand association by the ratios of the Stern−Volmer constants (Table 4). It is apparent that different ligands will induce different changes in the local environment in one PBP, and in different PBPs, different conformational changes are induced by the same ligand. A change in the ratio of the Stern−Volmer constants indicates that the environment around Trp is different, either electronically or sterically or both. Binding of PBP2 with (+)-disparlure has decreased the ratio by 62% but only by 45% for binding with NPN. On the other side, association with NPN has induced the biggest decrease of the ratio for PBP1. Besides the difference in the ligand-induced conformational change, kinetically, PBP1 interacts with ligand differently from PBP2. The backward reaction of step A between NPN and PBP2 is much faster than with PBP1.

The C-terminal peptide is important for PBP1 and PBP2 function. C-Terminal truncation of PBP1 caused the $k_{-A}$ value to increase in TPBP1. A similar comparison was not possible for PBP2 and TPBP2 because for both proteins the external binding was faster than the time resolution of the experiment. For both proteins, elimination of the C-terminal peptide resulted in a faster relaxation process for step B (Table 3, larger $k_{obs,B}$). In our previous paper about PBP2 and (+)-disparlure binding, TPBP2 displayed a slower unimolecular disparlure binding process (smaller $k_2$) (*12*). In this work, PBP1 and TPBP1 had similar binding affinities for NPN, but TPBP2 consistently bound ligand more weakly than PBP2 (Table 2 and ref *12*). PBP1 and TPBP1 exhibited different ratios of Stern−Volmer constants in different complexes, while PBP2 and TPBP2 had very similar ratios. Taken together, these data suggest that the C-terminal peptide plays different roles in PBP1 and PBP2. It is possible that the C-terminal peptide may also contribute to the PBP selectivity.

*Possible Function of Kinetic Steps*. We propose that there are different binding modes of the ligand on the PBPs: the encounter complex and two conformers of the PBP−ligand complex. One conformer may have lower energy than the other. Different conformers have been detected in the literature (see above). We hypothesize that these different binding stages/conformers of the P·L complex may serve different functions. Some conformers may have a specific (agonistic or antagonistic) effect on the OR signaling cascade (*5*, *29*, *30*). Other conformers may not affect the OR signaling, and these may serve as transporters or scavengers for the ligands (*6*).

The first collisional binding step and the corresponding reverse reaction are rapid, and they may aid hydrophobic ligands to remain in the aqueous lymph. The second binding step is also fast, and this step is on the correct time scale to be responsible for agonist or antagonist PBP conformers. The third step we detected previously (*12*) is too slow to account for any direct effects on the OR signaling cascade. It is, however, in the correct time regime to be responsible for ligand scavenging (Supporting Information ref *12*).

In conclusion, we have studied the interaction kinetics of PBP1 and PBP2 with one surrogate ligand, NPN. The results have provided further evidence of the stepwise interaction between PBP and a ligand and shown the possibility of a three-step binding model. The difference in affinity of NPN binding to PBPs between two different methods supports the hypothesis of the existence of multiple binding states of the PBP−ligand complex. Through a quenching study of the intrinsic fluorescence of Trp 37 with two quenchers of different inherent properties, we notice that the quenching profiles of PBPs with different ligands are unique (Table 4) and the change of the local environment around that residue happens immediately after the PBP and ligand are mixed (Figure 5). By comparing the binding properties of intact PBPs and TPBPs, we are able to further identify the importance of the C-terminal peptide of the long-chain PBPs. Besides acting as a gate for the ligand, it is also a distinct component of the PBP and may primarily help to discriminate ligands. We suggest that different kinetic steps may serve different PBP functions.

## ACKNOWLEDGMENT

We thank Dr. C. Castillo for PBP and TPBP preparation and X. Han (School of Engineering Science, Simon Fraser University, Burnaby, British Columbia) for helping with the preparation of the table of contents graphic.

## SUPPORTING INFORMATION AVAILABLE

NPN absorbance at different concentrations (Figure S1), comparison of the NPN or Trp fluorescence emission mixing with or in different PBPs (Figures S2 and S5), detailed explanation of the kinetic fitting procedure, the kinetics for mixing PBPs/TPBPs with NPN (Figures S3 and S4), and all Stern−Volmer constants used in this paper (Tables S1 and S2). This material is available free of charge via the Internet at http://pubs.acs.org.

## REFERENCES

1. Pesenti, M. E., Spinelli, S., Bezirard, V., Briand, L., Pernollet, J. C., Tegoni, M., and Cambillau, C. (2008) Structural basis of the honey bee PBP pheromone and pH-induced conformational change. *J. Mol. Biol. 380*, 158–169.
2. Damberger, F. F., Ishida, Y., Leal, W. S., and Wuethrich, K. (2007) Structural basis of ligand binding and release in insect pheromone-binding proteins: NMR structure of *Antheraea polyphemus* PBP1 at pH 4.5. *J. Mol. Biol. 373*, 811–819.
3. Lautenschlager, C., Leal, W. S., and Clardy, J. (2005) Coil-to-helix transition and ligand release of *Bombyx mori* pheromone-binding protein. *Biochem. Biophys. Res. Commun. 335*, 1044–1050.
4. Wojtasek, H., and Leal, W. S. (1999) Conformational change in the pheromone-binding protein from *Bombyx mori* induced by pH and by interaction with membranes. *J. Biol. Chem. 274*, 30950–30956.
5. Laughlin, J. D., Ha, T. S., Jones, D. N. M., and Smith, D. P. (2008) Activation of pheromone-sensitive neurons is mediated by conformational activation of pheromone-binding protein. *Cell 133*, 1255–1265.
6. Krieger, J., and Breer, H. (1999) Olfactory reception in invertebrates. *Science 286*, 720–723.
7. Honson, N., Johnson, M. A., Oliver, J. E., Prestwich, G. D., and Plettner, E. (2003) Structure-activity studies with pheromone-binding proteins of the gypsy moth, *Lymantria dispar*. *Chem. Senses 28*, 479–489.
8. Lautenschlager, C., Leal, W. S., and Clardy, J. (2007) *Bombyx mori* pheromone-binding protein binding nonpheromone ligands: Implications for pheromone recognition. *Structure 15*, 1148–1154.
9. Sandler, B. H., Nikonova, L., Leal, W. S., and Clardy, J. (2000) Sexual attraction in the silkworm moth: Structure of the pheromone-binding-protein-bombykol complex. *Chem. Biol. 7*, 143–151.
10. Kruse, S. W., Zhao, R., Smith, D. P., and Jones, D. N. M. (2003) Structure of a specific alcohol-binding site defined by the odorant binding protein LUSH from *Drosophila melanogaster*. *Nat. Struct. Biol. 10*, 694–700.
11. Lartigue, A., Gruez, A., Spinelli, S., Riviere, S., Brossut, R., Tegoni, M., and Cambillau, C. (2003) The crystal structure of a cockroach

pheromone-binding protein suggests a new ligand binding and release mechanism. *J. Biol. Chem. 278*, 30213–30218.
12. Gong, Y., Pace, T. C. S., Castillo, C., Bohne, C., O'Neill, M. A., and Plettner, E. (2009) Ligand-interaction kinetics of the pheromone-binding protein from the gypsy moth, *L. dispar*: Insights into the mechanism of binding and release. *Chem. Biol. 16*, 162–172.
13. Plettner, E., Lazar, J., Prestwich, E. G., and Prestwich, G. D. (2000) Discrimination of pheromone enantiomers by two pheromone binding proteins from the gypsy moth Lymantria dispar. *Biochemistry 39*, 8953–8962.
14. Lartigue, A., Gruez, A., Briand, L., Blon, F., Bezirard, V., Walsh, M., Pernollet, J. C., Tegoni, M., and Cambillau, C. (2004) Sulfur single-wavelength anomalous diffraction crystal structure of a pheromone-binding protein from the honeybee Apis mellifera L. *J. Biol. Chem. 279*, 4459–4464.
15. Mohanty, S., Zubkov, S., and Gronenborn, A. M. (2004) The solution NMR structure of *Antheraea polyphemus* PBP provides new insight into pheromone recognition by pheromone-binding proteins. *J. Mol. Biol. 337*, 443–451.
16. Wogulis, M., Morgan, T., Ishida, Y., Leal, W. S., and Wilson, D. K. (2006) The crystal structure of an odorant binding protein from *Anopheles gambiae*: Evidence for a common ligand release mechanism. *Biochem. Biophys. Res. Commun. 339*, 157–164.
17. Venyaminov, S. Y., and Vassilenko, K. S. (1994) Determination of protein tertiary structure class from circular-dichroism spectra. *Anal. Biochem. 222*, 176–184.
18. Fersht, A. (1999) Structure and mechanism in protein science: A guide to enzyme catalysis and protein folding, W. H. Freeman, New York.
19. Birks, J. B. (1970) Photophysics of aromatic molecules, Wiley-Interscience, New York.
20. Eftink, M. R., and Ghiron, C. A. (1976) Exposure of tryptophanyl residues in proteins—Quantitative determination by fluorescence quenching studies. *Biochemistry 15*, 672–680.
21. Lehrer, S. S. (1971) Solute perturbation of protein fluorescence—Quenching of tryptophyl fluorescence of model compounds and of lysozyme by iodide ion. *Biochemistry 10*, 3254–3263.
22. Bette, S., Breer, H., and Krieger, J. (2002) Probing a pheromone binding protein of the silkmoth *Antheraea polyphemus* by endogenous tryptophan fluorescence. *Insect Biochem. Mol. Biol. 32*, 241–246.
23. Leal, W. S., Chen, A. M., Ishida, Y., Chiang, V. P., Erickson, M. L., Morgan, T. I., and Tsuruda, J. M. (2005) Kinetics and molecular properties of pheromone binding and release. *Proc. Natl. Acad. Sci. U.S.A. 102*, 5386–5391.
24. Kowcun, A., Honson, N., and Plettner, E. (2001) Olfaction in the gypsy moth, *Lymantria dispar*—Effect of pH, ionic strength, and reductants on pheromone transport by pheromone-binding proteins. *J. Biol. Chem. 276*, 44770–44776.
25. Isin, E. M., and Guengerich, F. P. (2006) Kinetics and thermodynamics of ligand binding by cytochrome P450 3A4. *J. Biol. Chem. 281*, 9127–9136.
26. Honson, N. S., and Plettner, E. (2006) Disulfide connectivity and reduction in pheromone-binding proteins of the gypsy moth, *Lymantria dispar*. *Naturwissenschaften 93*, 267–277.
27. Vogt, R. G., Kohne, A. C., Dubnau, J. T., and Prestwich, G. D. (1989) Expression of pheromone binding-proteins during antennal development in the gypsy moth *Lymantria dispar*. *J. Neurosci. 9*, 3332–3346.
28. Thode, A. B., Kruse, S. W., Nix, J. C., and Jones, D. N. M. (2008) The role of multiple hydrogen-bonding groups in specific alcohol binding sites in proteins: Insights from structural studies of LUSH. *J. Mol. Biol. 376*, 1360–1376.
29. Grosse-Wilde, E., Svatos, A., and Krieger, J. (2006) A pheromone-binding protein mediates the bombykol-induced activation of a pheromone receptor in vitro. *Chem. Senses 31*, 547–555.
30. Pophof, B. (2002) Moth pheromone binding proteins contribute to the excitation of olfactory receptor cells. *Naturwissenschaften 89*, 515–518.